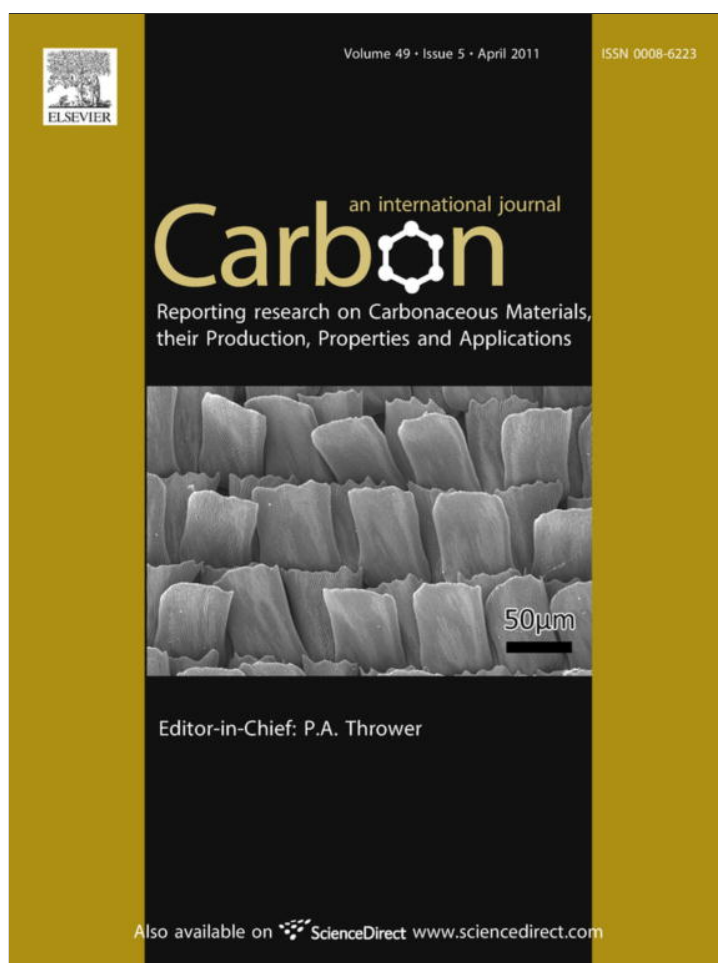


Provided for non-commercial research and education use.
Not for reproduction, distribution or commercial use.



This article appeared in a journal published by Elsevier. The attached copy is furnished to the author for internal non-commercial research and education use, including for instruction at the authors institution and sharing with colleagues.

Other uses, including reproduction and distribution, or selling or licensing copies, or posting to personal, institutional or third party websites are prohibited.

In most cases authors are permitted to post their version of the article (e.g. in Word or Tex form) to their personal website or institutional repository. Authors requiring further information regarding Elsevier's archiving and manuscript policies are encouraged to visit:

<http://www.elsevier.com/copyright>

available at www.sciencedirect.comjournal homepage: www.elsevier.com/locate/carbon

Thermophysical properties of multi-wall carbon nanotube bundles at elevated temperatures up to 830 K

Xiaopeng Huang ^a, Jianmei Wang ^{a,b}, Gyula Eres ^c, Xinwei Wang ^{a,*}

^a Department of Mechanical Engineering, Iowa State University, 2010 Black Engineering Building, Ames, IA 50011, USA

^b Department of Energy and Power Engineering, Wuhan University, PR China

^c Materials Science and Technology Division, Oak Ridge National Laboratory, 1 Bethel Valley Road, MS-6056, Oak Ridge, TN 37831-6056, USA

ARTICLE INFO

Article history:

Received 20 August 2010

Accepted 21 December 2010

Available online 24 December 2010

ABSTRACT

Thermal transport measurements in multi-wall carbon nanotube (MWCNT) bundles at elevated temperatures up to 830 K are reported using a novel generalized electrothermal technique. Compared with individual CNTs, the thermal conductivity (k) of MWCNT bundles is two to three orders of magnitude lower, suggesting the thermal transport in MWCNT bundles is dominated by the tube-to-tube thermal contact resistance. The effective density for the two MWCNT bundles, which is difficult to measure using other techniques, is determined at 116 kg/m³ and 234 kg/m³. The thermal diffusivity slightly decreases with temperature while k exhibits a small increase with temperature up to 500 K and then decreases. For the first time, the behavior of specific heat for MWCNTs above room temperature is determined. The specific heat is close to graphite at 300–400 K but is lower than that for graphite above 400 K, indicating that the behavior of phonons in MWCNT bundles is dominated by boundary scattering rather than by the three-phonon Umklapp process. The analysis of the radiation heat loss suggests that it needs to be considered when measuring the thermophysical properties of micro/nano wires of high aspect ratios at elevated temperatures, especially for individual MWCNTs due to their extremely small diameters.

© 2010 Elsevier Ltd. All rights reserved.

1. Introduction

Carbon nanotubes (CNTs) are attracting great attention because of their remarkable electrical, thermal, mechanical and optical properties [1]. To fundamentally understand the science of the thermal transport in CNTs, numerous experimental investigations have been conducted on the thermal properties of single-walled CNTs (SWCNTs) and multi-walled CNTs (MWCNTs) in various forms including films (arrays, bucky paper) [2–9], bundles [10–16], yarns and sheets [17], individual [11,18–21] and bulk [22–24] samples. The authors either measure the thermal conductance G or thermal conductivity k from the steady-state thermal transport process, or measure the thermal diffusivity α from the transient

thermal transport process. As a standard thermal property for comparison among researchers, the thermal conductivity k can be converted from G with known dimensions of the sample, and from α with the known density and specific heat of the sample. The reported values of the measured k at room temperature vary from 300 to 3500 W/m K for an individual tube, either single-walled or multiwalled, and 3–150 W/m K for the tube direction of bulk CNT samples except a scaled-up value 200 W/m K in Ref. [2].

The significant diversity of the experimental results is mainly due to differences in various parameters and samples conditions, such as diameter (inner and outer diameter for MWCNTs), length, defects and deformations in individual tubes, purity, alignment, fabrication method and post growth

* Corresponding author. Fax: +1 515 294 3261.

E-mail address: xwang3@iastate.edu (X. Wang).

0008-6223/\$ - see front matter © 2010 Elsevier Ltd. All rights reserved.

doi:10.1016/j.carbon.2010.12.053

treatment for bulk CNTs. The density and specific heat of CNT samples also introduce differences due to different assumptions for them or the disparity of the measured values of different samples. For the density, several authors assumed that the bulk samples including bundles and arrays have the same density as graphite at about 1580–1900 kg/m³ [4,6,10]. Actually, the density of a disk-shape MWCNT fabricated by spark plasma sintering (SPS) from 800 to 2000 °C can be densified from 350 to 1450 kg/m³ [22]. The apparent densities of aligned and random bucky papers were calculated at 620 and 540 kg/m³ by measured weight and dimensions, respectively [7]. Our previous work [15] also reported a density of 310 ± 40 kg/m³ for MWCNT bundles calculated by measured thermal conductivity and thermal diffusivity. The effective density of vertically aligned CNT array is directly fitted from the experimental curve as 185 kg/m³ [5]. Therefore, the disparity of the density among samples contributes to the diversity of the reported thermal conductivity. As for the specific heat c_p , it has been reported that a linear temperature dependence of the normalized c_p of MWCNT between 150 K and 300 K is similar to graphite with a smaller absolute value of c_p at 300 K [10]. Other reported graphite-like $c_p(T)$ of MWCNT below room temperature [25,26] also strongly suggested that the specific heat behavior of the bulk MWCNT is very similar to that of graphite with the same 300 K value. Therefore, it is reasonable to take the specific heat of graphite [27] for CNT at corresponding temperatures below 300 K. However, there is no strong evidence that CNT materials and graphite have the same behavior on specific heat above 300 K. Additionally, the Debye temperature for CNTs which can be used to theoretically estimate $c_p(T)$ in the entire temperature range is not completely clear, although it is expected to be similar to that of graphite [28]. Therefore, more research should focus on the specific heat of MWCNTs at high temperatures.

The temperature dependence of thermal conductivity is a critical characteristic of CNTs for a wide range of applications. A significant amount of experimental research has already been conducted on this. Examples include the work on individual MWCNT at 100–320 K [18], individual SWCNT at 100–300 K [19] and 300–800 K [20], individual and bundled MWCNT at 8–370 K [11], MWCNT bundles at 10–300 K [10,14], MWCNT arrays at 5–390 K [9], 90–310 K [3] and 218–473 K [6], aligned thin films of SWCNT ropes at 10–400 K [2], bulk disk-shape MWCNT at 328–958 K [23], and CNT bars at 2–300 K [24]. The results for both individual SWCNTs and MWCNTs indicated a peak k at about 320 K. All these experimental results showed k - T is a gradually increasing curve for bulk CNTs except that a peak was found at near 900 K for disk-shape MWCNTs measured by the laser flash method [23]. It should be pointed out that the radiation heat loss is very critical for high temperature measurement in laser flash method due to the large radiation surface area of a disk sample [29]. Possibly it is the reason for the decrease after 900 K in the k - T curve. Computational methods, especially molecular dynamics simulation, were also employed by many researchers to investigate the k - T relation for CNTs [30,31]. However, there is no consistent and convincing conclusion on it especially in the elevated temperature range. Little experimental research was conducted on the thermal conductivity of CNTs

at elevated temperatures above 400 K. Therefore, further study of k - T of CNTs at elevated temperatures is needed.

High temperature annealing in Ar environment will affect the electrical and thermal conductivity of MWCNT bundles in the way which depends on the competition of dopants removing and carriers moving enhancement [14]. Recently, resistance reduction of carbon nanofibers was also observed due to electrical current annealing [32]. Electrical current annealing in graphene can also result in removal of adsorbates [33] and electron-hole conduction asymmetry [34]. Due to the cross contact of individual tubes in CNT bundles, it is also possible that current tunneling effect occurs at a certain level and the thermal properties may be affected. Hence, it is an interesting question that if current annealing process or real-time feeding current upon CNT bundles will change the tube-to-tube contact and then affect the electrical and thermal conductivity permanently or temporarily.

In this paper, the temperature and electric current dependence of the thermal diffusivity, thermal conductivity, and specific heat of MWCNT bundles at elevated temperatures are investigated by using generalized electrothermal (GET) and pulsed laser-assisted thermal relaxation (PLTR) [16] techniques with calibration of the temperature coefficient of CNT's resistance. The experimental details of the GET technique and the calibration are given in Section 2. In Section 3, the results are discussed and compared with those in the literature. The thermal contact resistance and effects of radiation heat loss, which are critical issues in thermal property measurement of micro/nano-scale materials, are also discussed in detail.

2. Experimental principles and details

2.1. Generalized electrothermal (GET) technique: transient and steady states

The transient electrothermal (TET) technique was developed by Guo et al. [13] to measure micro/nano-scale wires. It can be applied to metallic, semiconductive and nonconductive materials and is featured with strong signal level and instant measurement results. In the original development, the TET technique only measures the thermal diffusivity α of wire samples from the transient phase of the electrothermal process, and the thermal conductivity k can be calculated from $\alpha = k/\rho c_p$ if the density ρ and specific heat c_p are known. In the present work, the steady-state of the electrothermal process is utilized to directly determine k with calibration of the temperature coefficient of resistance without known density and specific heat. These two processes are combined to obtain α and k simultaneously at a wider range of temperature. To distinguish it from other electrothermal techniques using infrared [7] or Raman signal [15] for thermal sensing, this combined technique probing the temperature with self-resistance monitoring is termed the generalized electrothermal (GET) technique. Although the principle of the GET technique is similar to the bridge method, the bridge method is originated from measuring the in-plane thermal properties of thin film and it always considers the radiation effect due to the large surface-to-volume ratio. In addition, the temperature

increase evolution was experimentally observed by the previous developer and evaluated with an approximation equation in the bridge method. Furthermore, the thermal diffusivity is calculated by the characteristic point method. The GET technique was developed targeting micro/nanowires and the radiation effect can be neglected except at high temperatures. An exact analytical solution to the 1-D heat transfer in the GET technique is provided and a global fitting of the experimental curve is used to obtain the thermal diffusivity more accurately [12].

In the TET technique, the to-be-measured wire (treated as 1-D) is suspended between two electrodes, which have very high thermal and electrical conductivities to be good heat sinks (as shown in Fig. 1a). The α information about the wire is involved in its temperature evolution under a given self-heating power. Simplifying with $\Theta(t, x) = T(t, x) - T_0$, the solution of this 1-D heat transfer problem is [13]

$$\frac{\bar{\Theta}(t)}{\bar{\Theta}(\infty)} = \frac{96}{\pi^4} \sum_{m=1}^{\infty} \frac{1 - \exp[-(2m-1)^2 \pi^2 \alpha t / L^2]}{(2m-1)^4}, \quad (1)$$

where $\bar{\Theta}(t) = \int_0^L \Theta(t, x) dx / L$ denotes the average temperature of the wire at time t , $\bar{\Theta}(\infty)$ the final steady-state average temperature which is $\dot{q}L^2/12k$, \dot{q} the electrical heating power per unit volume, L the length of the wire between the two

electrodes, and T_0 the initial temperature of the wire. From Eq. (1), for any kind of wire samples with any length, they have the same normalized temperature increase curve with respect to the Fourier number $Fo = \alpha t / L^2$. It should be mentioned that the self-heating power needs to be maintained constant to make the solution valid. A step DC current fed through the wire is applied in this technique in which the fluctuation of the heating power could be neglected due to minor variation of the wire resistance. If the sample has a linear relationship between resistance and temperature in a small temperature range near the initial temperature T_0 , meaning a constant temperature gradient of resistance $R' = \beta R_0 = [\Delta R(t) / \bar{\Theta}(t)]_{T_0}$ referring β as the temperature coefficient of resistance at T_0 , we have $\bar{\Theta}(t) / \bar{\Theta}(\infty) = \Delta R(t) / \Delta R(\infty) = \Delta V(t) / \Delta V(\infty)$ with constant DC current. After measuring and normalizing the voltage variation against time over the sample, the thermal diffusivity can be obtained by fitting that curve with the theoretical one represented by Eq. (1). Actually, to determine the thermal diffusivity of the sample, the values of R' and \dot{q} are not needed and it is sufficient that they are constant. However, in realistic experiments, the signal level $\Delta V(\infty)$ available to be captured is a major concern. Previous discussion indicates $\Delta V(\infty) = I \Delta R(\infty) \propto I \dot{q} \propto I^3$ and $\bar{\Theta}(\infty) \propto I^2$. A high current gives a strong signal as well as a large temperature variation which introduces large uncertainty caused by non-constant heating power and temperature-dependent thermal conductivity. Therefore, to minimize the uncertainty, it is best to achieve a reasonable signal-to-noise ratio with the current as low as possible.

The thermal conductivity k cannot be obtained from α measured by the TET technique without knowing ρ and c_p . In this work, an extension of the TET technique, the GET technique, is developed to obtain k from room temperature to high temperatures without knowing ρ and c_p . It should be noted that k appears in the steady-state average temperature increase as $\bar{\Theta}(\infty) = \dot{q}L^2/12k$. Combined with $R' = \Delta R(\infty) / \bar{\Theta}(\infty)$, k can be calculated as $\dot{q}L^2 R' / 12 \Delta R(\infty)$ with knowing the value of \dot{q} and R' , in which $\Delta R(\infty) = \Delta V(\infty) / I$. \dot{q} can be calculated as $I^2 R_0 / A_c L$ with the assumption that the resistance variation is negligible for the heating power, in which A_c is the cross-sectional area of the wire. R' can be obtained from references or calibrated by experiments. With α obtained from the transient process and k obtained from the steady-state process in this GET technique, plus the known specific heat, the density of the wire can also be determined. In this work, a two-step DC current input as shown in Fig. 1b is introduced to investigate the effect of current on the thermal properties of CNT bundles and at the same time extend the GET technique to measure k at elevated temperatures. Due to the linearity of the governing partial differential equation of this 1-D heat transfer problem, the two-step self-heating current case has a linearly combined solution of each solution for the one-step current case described above. The first step current, termed base current I_b , heats the wire to a high base temperature, and the second step current, termed probing current I_p , heats the wire up as low as possible and probes the temperature evolution to obtain k , just as in the GET technique with only a one-step current (GET 1). The high base temperature can be calculated from the steady-state solution $\bar{\Theta}(\infty) = \dot{q}L^2/12k$ of the first step self-heating after having the thermal

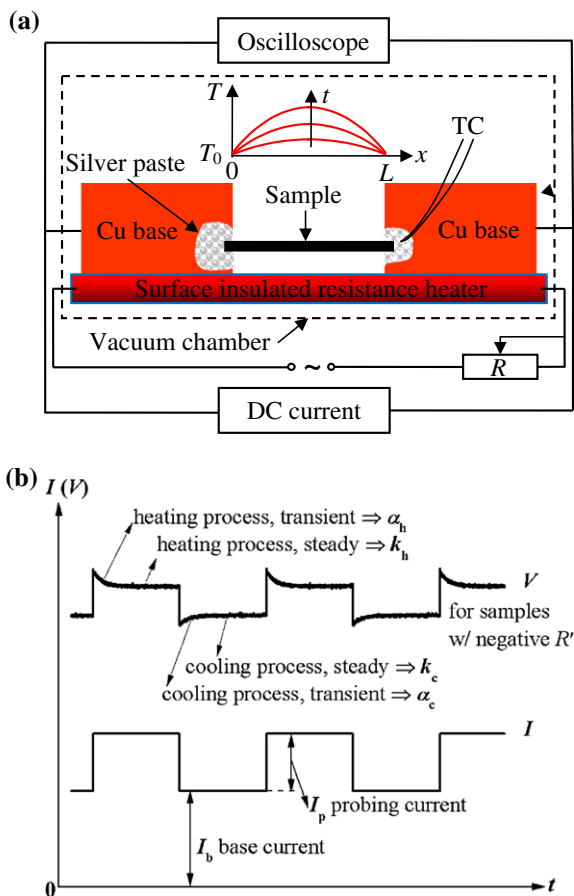


Fig. 1 – (a) The schematic of the experimental setup and the typical temperature profile history of the wire sample, (b) The typical two-step input DC current signal and output voltage signal for the GET 2 technique.

conductivity from the steady-state solution of the second step self-heating.

2.2. Experimental setup

The schematic of the experimental setup and a typical temperature profile history are given in Fig. 1a. The sample is suspended between two copper block electrodes and the two joints are glued with silver paste to reduce both the thermal and electrical contact resistances. The entire stage with the sample is placed on a surface insulated joule heater that is controlled by an external adjustable transformer. The heater is used to heat the entire stage to a stable temperature and the temperature is sensed by a T-type thermocouple. This setup is housed in a vacuum chamber with the pressure below 1×10^{-3} Torr to make the heat convection negligible. A two-step DC current is fed through the sample by a current source to induce electrical heating. At the same time, the voltage variation over the sample is recorded by an oscilloscope. A typical input current signal and output voltage signal are shown in Fig. 1b. The base current I_b in the first step is to heat the sample to a certain temperature, and the probing current I_p in the second step is to heat the wire up as low as possible and probe the temperature evolution to obtain k . A periodic current is applied to repeat the measurement and make the output signal easily be recognized and captured. Due to this periodic characteristic, the first step actually has a cooling process after the probing current is done. This cooling process is just a reversed process of heating the sample with the power $[(I_b + I_p)^2 - I_b^2]R_0$ and sensing temperature evolution with I_b as in the GET 1 technique. The thermal properties α_c and k_c can also be respectively obtained from the transient and steady stages of this process. These provide the information for comparison and more understanding of the electro-thermal coupling process in the sample.

2.3. Experimental details

The two samples investigated in this work are bundles from a 3.5 mm long MWCNT rope. One is a thin and long bundle peeled off the rope, and the other one is a thick and short bundle cut from it. The MWCNT ropes were synthesized using a ferrocene assisted chemical vapor deposition (CVD) process in quartz tube furnace. Except using a patterned catalyst area for defining the diameter of the bundle, the details of the synthesis process were described in the literature [35]. Briefly, the catalyst consists of a 100 nm Al and 1 nm Fe layer deposited on a Si wafer using electron beam evaporation through a shadow mask with periodic holes of 200 μm in diameter. Acetylene was used as the carbon source gas, and it was flowed concurrently with ferrocene sublimated from a thermal source in the CVD process. Single $\sim 200 \mu\text{m}$ diameter MWCNT ropes were harvested from a large area sample for the thermal properties measurements. The diameter of real samples may be a little larger than 200 μm due to the bundle loosing after being exposed in the air. The Raman spectra of a typical MWCNT bundle at five different locations are shown in Fig. 2a. They were taken with a 532 nm (2.34 eV) laser excitation wavelength at 20 mW energy output. The D-band and G-band are at 1346 cm^{-1} and 1577 cm^{-1} . The average D–G

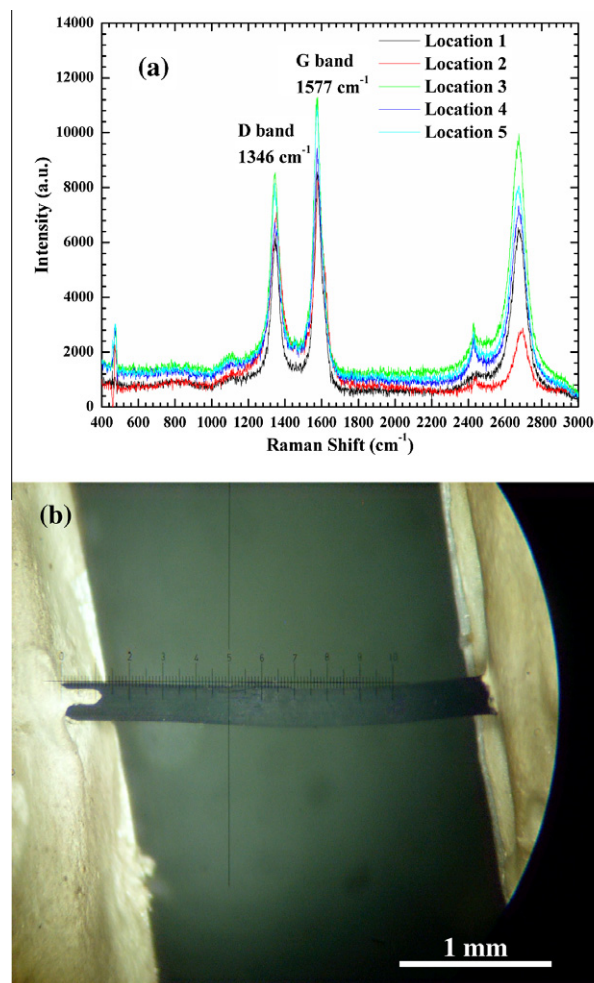


Fig. 2 – (a) Raman Spectra of a typical MWCNT bundle at five different locations taken with a 532 nm (2.34 eV) laser excitation wavelength at 20 mW energy output. (b) Picture of the second MWCNT bundle ($L = 2.90 \text{ mm}$, $D = 233 \mu\text{m}$) under an optical microscope (glued on the electrodes with silver paste).

band intensity ratio is 0.73. The diameter of the bundle sample from the rope is measured by using a high magnification microscope (Olympus BX41). The second thick MWCNT bundle is picked to show what the real sample looks like when it is glued on the electrodes with silver paste. Fig. 2 shows its image under an optical microscope. To capture the transient voltage variation in the GET experiment, the current source should have very small rise time compared with the characteristic thermal transport time (milliseconds to seconds) of a wire sample. A current supply – Keithley 6221 with 2 μs rise time and 100 mA maximum output current is used for the thin bundle sample whose resistance is in the order of one hundred ohms, and Keithley 2611 with 70 μs rise time and 1.5 A maximum output current for the thick bundle sample which has a small resistance in the order of ten ohms. The voltage evolution is monitored and recorded using a Tektronix TDS7054 Digital Phosphor Oscilloscope which has a maximum sampling rate of 5 GS/s. Since the CNT sample has a negative temperature coefficient of resistance, the

output voltage decreases in the heating process and increases in the cooling process, as shown in Fig. 1b. With a suitable probing current I_p , cross-measuring the response of different base currents I_b at different stable temperatures T_0 produces the thermal properties at different temperatures. This is because the temperature gradient of resistance R' can be obtained from the resistances at difference temperatures for a certain I_b and then all the voltage variations can be converted to temperature variations, which can help determine the thermal conductivity. The thermal diffusivity is obtained by fitting the normalized temperature evolution curve against time to the theoretical curve represented by Eq. (1) with a robust program [13].

In order to investigate the annealing effect which may occur due to the periodical one-step/two-step current heating, the GET technique with a one-step current (GET 1) is applied while gradually increasing the current from a low value to a high one for a few cycles. After excluding the possible annealing effect in the experiments, the electrothermal technique with a two-step current (GET 2) is applied to the sample. For the first long and thin bundle (3.33 mm long and 94.5 μm diameter), to study the annealing effect, a current from 2 mA to 30 mA is applied with GET 1. In the following process with GET 2 at room temperature, the probing current is fixed at 2 mA and the base current varies from 1 mA to 28 mA. In calibration, the entire sample is heated to a higher temperature up to 100 $^{\circ}\text{C}$, and one-step currents from 0 mA to 30 mA are applied and the output voltage histories are recorded at each stable temperature. A MWCNT bundle with a larger diameter and sound circular cross-section (2.90 mm length and 233 μm diameter) is chosen as the second sample for measurement at higher temperatures. To avoid the annealing effect, this sample is applied with one-step current from 16 mA to 320 mA for two cycles. The resistance is then measured in the vacuum chamber as 9.276 Ω . After these, the GET 2 technique is applied. The sample is heated up to 300 $^{\circ}\text{C}$. At each temperature, the probing current I_p is chosen at 10 mA and the base current I_b scans from 20 to 300 mA.

3. Results and discussion

3.1. MWCNT bundle with $L = 3.33$ mm and $D = 94.5$ μm

Fig. 3a shows a typical experiment voltage evolution signal with 6 mA base current and 2 mA probing current at room temperature for this MWCNT bundle. Periodic heating (decreasing voltage) and cooling (increasing voltage) processes are obviously observed in the figure. The inset shows the global fitted experimental and theoretical curves of the normalized average temperature evolution for one of the heating processes. The least square fitting has a very small deviation. The thermal diffusivity is obtained at $6.10 \times 10^{-5} \text{ m}^2/\text{s}$. In the annealing process applying with from 2 mA to 30 mA, 4 mA is the minimum current which can produce applicable voltage variation signal. Our later analysis indicates that 4 mA current can induce 5 K (typical) increase for the maximum temperature (in the middle point of the wire sample), with $\bar{\Theta}(\infty) \propto I^2$, 30 mA current will increase the temperature by 281 K and the maximum temperature is

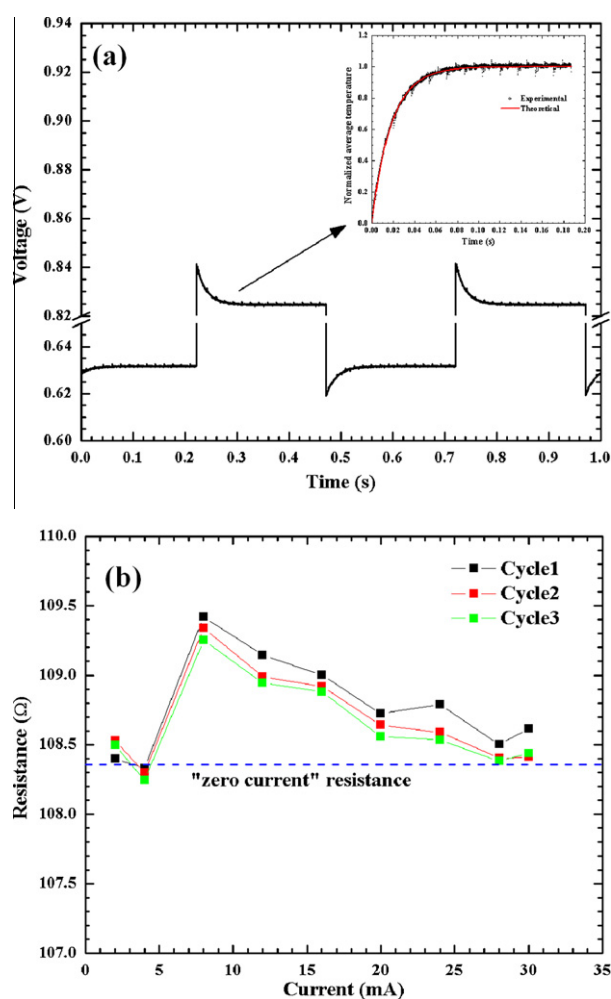


Fig. 3 – (a) A typical experiment voltage evolution signal with 6 mA base current and 2 mA probing current at room temperature for the first MWCNT bundle (3.33 mm long and 94.5 μm thick). Periodic heating (decreasing voltage) and cooling (increasing voltage) processes are obviously observed. The inset shows the global fitted experimental and theoretical curves of the normalized average temperature evolution for one of the heating cycles. (b) The resistance obtained in the GET 1 technique with the current from 2 mA to 30 mA for three cycles, in order to investigate the current annealing effect. The effect is noticeable and disappears after 2 cycles of current annealing.

still below the breakdown temperature 800 K for CNTs in air [20]. With the assumption that the electrical heating power is constant at one current and then fitting experiment curve with the theoretical curve represented by Eq. (1), the thermal diffusivity basically increases with the current. However, $\alpha(I)$ curve is not presented here because the calculated thermal diffusivity at high temperature is higher than the true value due to the large decrease of resistance under high temperature. Moreover, the slightly lower thermal diffusivity for the low currents in cycle 1 and the same value for each current in the next two cycles indicate that a slight annealing effect occurs under the currents below 24 mA in the first cycle and it is permanent. The annealing process changes the structure

in the CNTs such as tube end–end contact, tube body–body contact and tube body–end contact. These three kinds of contact affect the thermal transport in different ways which are related to the alignment of the CNTs. Briefly, the thermal diffusivity is enhanced after the annealing. Electrical properties are also a major concern when a CNT material is fabricated. The annealing effect and the current fed through the sample may also influence the electrical properties of CNTs. The resistance under each current at room temperature before heating is plotted in Fig. 3b. The “zero current” resistance is measured under very low current (μA) in the vacuum chamber before the GET experiments. The result shows that the resistance is close to the “zero current” resistance at small currents, and after a short increase it decreases roughly linearly above 8 mA current. The measurements on several test samples before this measurement also give the results about the curve of resistance against current that there is a small increase part before it decreases linearly. The differences for several samples are the currents at which the resistance begins to decrease and the decrease extent. The likely explanations for this phenomenon are as follows: (1) as the current increases from a very small value, more electrons flow through each individual CNT in the bundle. Due to the small diameter of an individual CNT, the electron boundary scattering is enhanced when more electrons flow in the sample, which means an increase of resistance; (2) as the current increases further, the enhancement of electron boundary scattering becomes weak. On the other hand, considerable tube-to-tube junctions begin to carry currents due to the current tunneling effect. This effect contributes to the resistance decrease. The lower resistances in the second and third cycles indicate that the periodic heating and cooling processes induced by one-step DC current has a slight effect on the resistance and the effect becomes negligible after two cycles.

The results of the GET 2 measurement show that the steady-state resistance at each current linearly decreases with the temperature. The slope of the linear curve R' is negative and increases with the current as shown in Fig. 4a. The reason for the increase is that the steady-state resistance R_0 decreases with the current due to the increasing self-heating power and resistance reduction. With the calibrated R' , the thermal diffusivity and thermal conductivity against the base current are calculated and shown in Fig. 4b. The thermal diffusivity of $5.5\text{--}7 \times 10^{-5} \text{ m}^2/\text{s}$ and thermal conductivity of $5\text{--}8.5 \text{ W/m K}$ for this MWCNT bundle have the same order of magnitude as those of MWCNT bundles [10,16], spark plasma sintered bulk MWCNT [22,23], aligned MWCNT arrays [3,4], and CNT bars [24]. At the same time, they are two to three orders of magnitude lower than the experimental and theoretical values of individual CNTs.

Basically, the thermal diffusivity does not vary with the current much except a slight increase at large current. The small difference (<5%) between the thermal diffusivity obtained from the transient heating and cooling processes is probably due to the relatively lower signal-to-noise ratio in the cooling step. For the thermal conductivity from the two processes, the difference is smaller because the error introduced by the noise is almost removed by averaging data from the steady state. From Fig. 4b we can see that the thermal conductivity increases with the current. Because the base

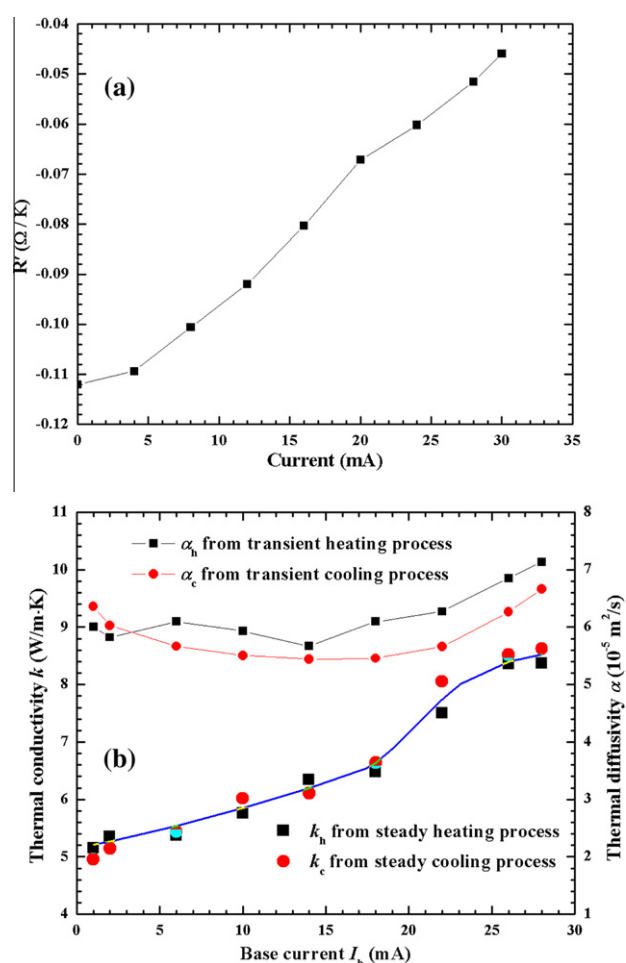


Fig. 4 – (a) The temperature gradient of resistance as a function of current. (b) The thermal diffusivity and thermal conductivity measured at different base currents. The solid blue line is a guide to the eye.

current heats the sample to a high temperature, these curves may reflect the temperature dependence of the thermal properties. Actually, the temperature dependence of the thermal properties can be obtained from the calibration data (GET 1) at different temperatures for a minimal current with a good signal-to-noise ratio. It is found that the data of 4 mA current produces sound results with low uncertainties. These data give a slightly increasing temperature dependence curve for k and a slightly decreasing temperature dependence curve for α in the range of $20\text{--}100^\circ\text{C}$, as shown in Fig. 5a. Based on estimation for GET 2 data, 11 mA current can heat the sample to about 100°C . Comparing k and α in Fig. 5a obtained from GET 1 data of $20\text{--}100^\circ\text{C}$ and in Fig. 4b from GET 2 data of $4\text{--}11 \text{ mA}$ base current, they agree with each other well. To have a wider comparison, the stage temperature should be higher. These measurements were performed on the second sample and will be discussed later.

Since $\alpha = k/\rho c_p$, the density ρ can be estimated which is not easy to measure using other techniques. As discussed in Introduction, it is reasonable to take the specific heat of graphite for CNT below 300°C . Thus, after taking an interpolated value $c_p(24^\circ\text{C}) = 704.4 \text{ J/kg K}$ from Ref. [25], the effective

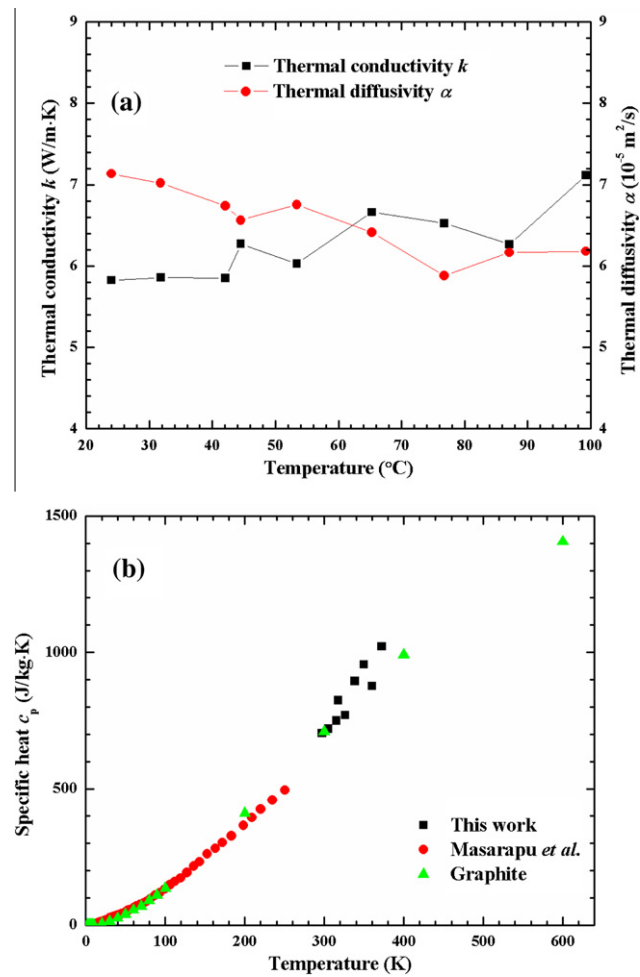


Fig. 5 – Temperature dependence of the thermophysical properties of the first MWCNT bundle: (a) thermal diffusivity α and thermal conductivity k ; (b) specific heat c_p .

density of this MWCNT bundle at 24 $^{\circ}\text{C}$ is calculated at 116 kg/m^3 , which is one order lower than the bulk density of MWCNT at $\sim 1600 \text{ kg}/\text{m}^3$ from other work [36] and is in the same order of the density 234 kg/m^3 [3] and 185 kg/m^3 [5] of aligned CNT arrays. Actually, a MWCNT sheet can be densified from 1.5 kg/m^3 to 600 kg/m^3 [37] and a disk-shape MWCNT sintered from 800 to 2000 $^{\circ}\text{C}$ can also be densified from 350 to 1450 kg/m^3 [22]. Thus, our reasonable low value of the density indicates that the sample was fabricated with a low packing fraction. The peeling process from a MWCNT rope may also make the sample a little loose. The low packing fraction guarantees that the change of the apparent bundle diameter in the vacuum due to thermal expansion is negligible even at high temperatures. Thus, it is proper to assume the density is constant during the whole measurement, which is also the assumption Yi et al. made when they concluded the linear specific heat of MWCNT at 10–300 K after measuring k and α by the 3ω method [10]. With this assumption, the specific heat above room temperature is calculated and is shown in Fig. 5b. For comparison, $c_p(T)$ of graphite and MWCNTs [26] are also plotted in the figure. It is seen that the behavior of $c_p(T)$ for MWCNTs is still close to graphite at 300–400 K. A wider comparison will be presented later with respect to the other sample.

The pulsed laser-assisted thermal relaxation (PLTR) technique is another suitable method to measure the thermal properties of wires and thin films at micro/nano-scales with fast experiment implementation and high signal-noise ratio [16]. In this work, the PLTR technique is also employed to provide a benchmark for the GET 2 technique. Besides the same equipment and experiment setup as in the GET 2 technique, a Nd:YAG laser operated with a 7 ns pulse width is used to heat the sample. The measurements with different DC currents as those used in the GET 2 technique are performed and both results are shown in Fig. 6. Both curves reveal a similar tendency and a small oscillation is observed in the PLTR curve due to the relatively large uncertainty. The PLTR results are a little lower than the GET 2 results for all currents. It should be mentioned that this PLTR measurement was performed half a day later after the GET 2 measurement. A slight structure change like tube-to-tube breakdown and tube breaking inside can increase the thermal resistance because the temperature at the tube-to-tube junctions reaches the burning temperature of CNTs at high stage temperature and high current during the GET 2 measurement. Taking the extreme case for example, in the last measurement of the calibration process, the highest current 30 mA was fed through the sample at the highest temperature 100 $^{\circ}\text{C}$. The maximal temperature at the middle of CNT bundle can be calculated at $\sim 800 \text{ K}$ by $(\dot{q}L^2)/8k$, in which the resistance used to calculate heating power is chosen at 80 Ω , a value between the before-heating and after-heating resistances, and k is chosen at 8 $\text{W}/\text{m K}$ from previous results. Considering the fact that most part of the heat is first generated at the tube-to-tube junctions due to their large contact resistance, it is very possible the maximal temperature exceeds 1000 K, which is close to the thermal oxidation temperature of CNTs at 800–900 K in air and $\sim 1200 \text{ K}$ in N_2 gas. This will result in the tube-to-tube breakdown. In addition, the extra vacuum pumping and sample stage movement may also lead to some tube bending and breaking.

3.2. MWCNT bundle with $L = 2.90 \text{ mm}$ and $D = 233 \mu\text{m}$

Fig. 7a shows the thermal diffusivity from the transient heating stage at different temperatures and different currents. It is observed the current only has a negligible effect on the thermal diffusivity. From room temperature to 200 $^{\circ}\text{C}$, the thermal diffusivity stays at $4.2 \pm 0.3 \times 10^{-5} \text{ m}^2/\text{s}$. At temperatures above 200 $^{\circ}\text{C}$, α decreases to $2.8 \pm 0.2 \times 10^{-5} \text{ m}^2/\text{s}$ at 240 $^{\circ}\text{C}$ and $2.4 \pm 0.4 \times 10^{-5} \text{ m}^2/\text{s}$ at 280 $^{\circ}\text{C}$. The steady-state resistance values under the base currents at different temperatures are used to calculate the temperature gradient of resistance. In this calibration process, it is observed that all the steady-state resistances under different base currents at temperatures above 200 $^{\circ}\text{C}$ are abnormal. For each base current, the steady-state resistance smoothly decreases with temperatures below 200 $^{\circ}\text{C}$ and then has an unexpected jump above 200 $^{\circ}\text{C}$. Considering the sudden drop of the thermal diffusivity at high temperatures above 200 $^{\circ}\text{C}$ shown in Fig. 7a, it is believed that the sample undergoes some structural change at high temperatures which can reduce α significantly. Probably there is tube-to-tube junction burning caused by powerful self-heating as previously described, or tube breaking induced

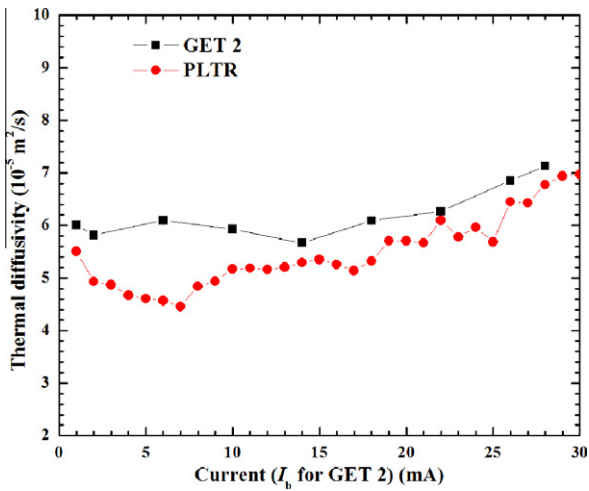


Fig. 6 – The thermal diffusivity at different base currents obtained from both the GET 2 and PLTR techniques.

by a considerable stress along with the noticeable thermal expansion of the block electrode at high temperatures. Therefore, the steady-state resistances at temperatures over 200 °C are not used for calibrating the temperature gradient of resistance. Actually, the resistance does not ideally decrease linearly with the temperature within the range of 26–200 °C. There is a slight up-deviation from the linear curve at high temperatures. Considering the high sensitivity of R' to k , the $R(T)$ curve is fitted to a parabolic curve with least square fitting and then R' is calculated at each temperature. As a result, every temperature at every current has an individual R' and k is then obtained with them as shown in Fig. 7b. The results indicate no obvious increase or decrease for $k(I_b)$ and $k(T)$ and hence k is statistically calculated as 8.6 ± 0.4 W/m K at 26–200 °C and 20–300 mA.

Although the data for α and k at different temperatures is shown in Fig. 7, they deserve separate plots to clearly see the relationship. Although the base current has a negligible effect on thermal transport in the sample, it heats the sample up. Thus, α and k obtained at a stage temperature and a base current are actually the ones at the temperature which has the extra temperature rise caused by the base current. This extra temperature rise can be calculated as $I^2 R_0 L / 12 A_c k$. k used in this calculation is the thermal conductivity obtained in the corresponding stage temperature and base current. This calculated temperature rise is a little lower than the actual one due to the low estimation of the heating power using the decreased steady-state resistance. After this procedure, the thermal properties α and k at temperatures up to about 830 K are obtained, as shown in Fig. 8a. It indicates that α decreases and k increases slightly with the temperature. Many literatures have reported that α of bulk CNT materials measured by different techniques does not vary with temperature much from 100 K to 470 K [3,6,10] and k almost increases linearly with temperature below 300 K [2,10,24]. In our result, the maximum α decrease is about 12% from 300 K to 830 K and this percentage level is neglected in other experiments [3]. Above 300 K, k still increases, but the increasing rate obviously becomes slower. Only 9.3% increase from 300 to 400 K

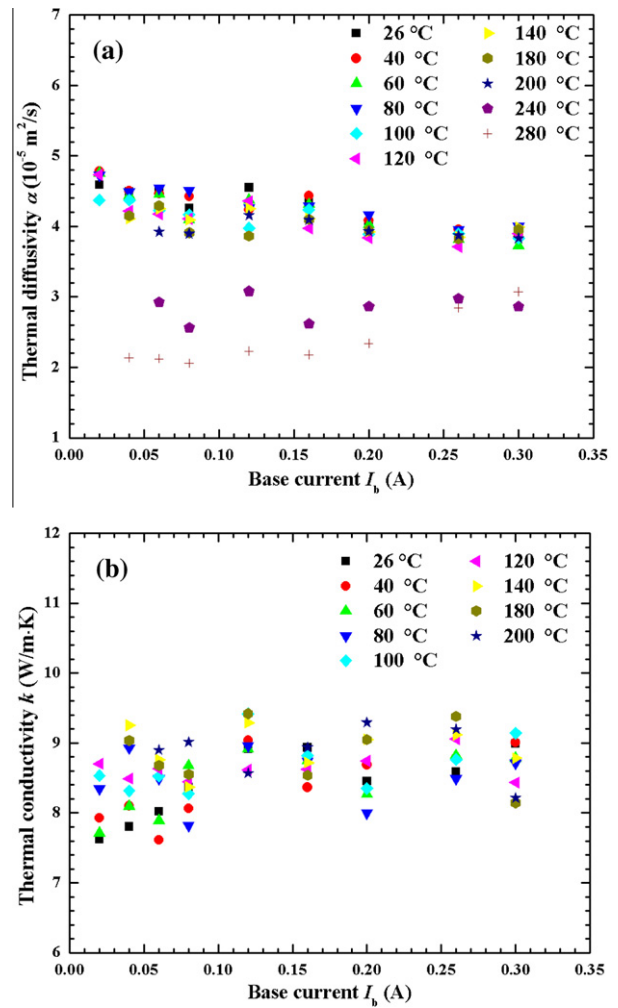


Fig. 7 – The thermophysical properties from the heating process at different temperatures and currents. (a) The thermal diffusivity α is $4.2 \pm 0.3 \times 10^{-5}$ m²/s at 26–200 °C, $2.8 \pm 0.2 \times 10^{-5}$ m²/s at 240 °C and $2.4 \pm 0.4 \times 10^{-5}$ m²/s at 280 °C, respectively. The very possible reasons for the lower α at temperatures above 200 °C are the structure change in the sample caused by the junction burning and the thermal expansion of the block electrode. (b) The thermal conductivity k remains constant at 8.6 ± 0.4 W/m K. Considering the structural changes above 200 °C, the resistance cannot be used for R' calibration and hence, k at these temperatures cannot be obtained.

for an aligned thin film of SWCNT ropes was reported [2], which is similar to our 15% increase for a MWCNT bundle. The k increase above 300 K indicates that the dominant phonon scattering mechanism at high temperatures is boundary and point-defect scattering rather than the three-phonon Umklapp scattering in many bulk solid materials which results in a decreasing k at high temperatures. The effect of radiation on measurement at high temperatures will be discussed later.

With $c_p(300 \text{ K}) = 709$ J/kg K, the effective density is calculated at 234 kg/m³ from $k/\alpha c_p$ with the measured k and α , about twice the density of the first peeled sample. The possible reasons for the difference are (1) the cross-section of the

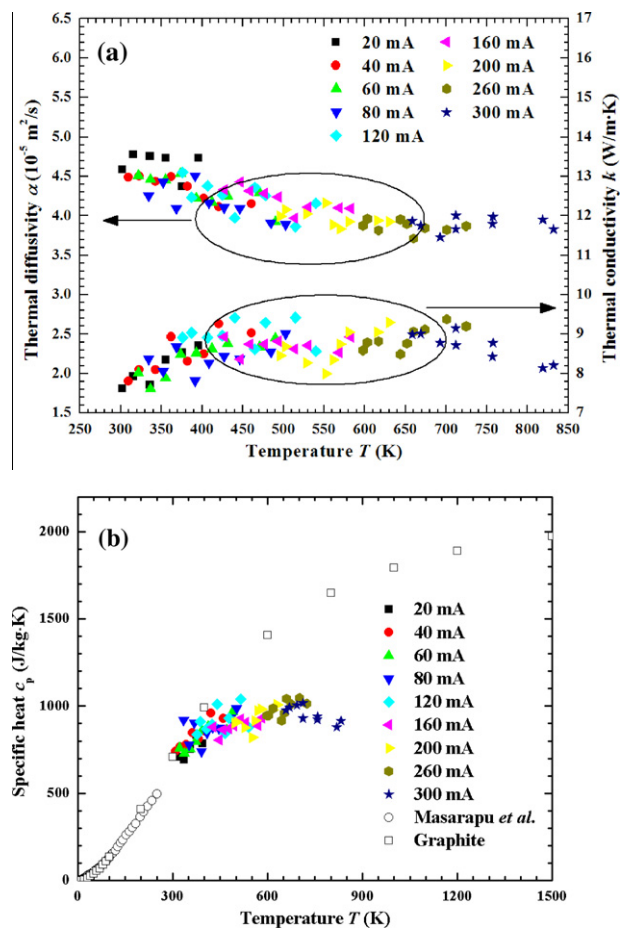


Fig. 8 – Temperature dependence of the thermal properties of the second MWCNT bundle: (a) thermal diffusivity α and thermal conductivity k , the measured values at high temperatures are slightly overestimated due to the radiation heat effect; (b) the lower specific heat c_p values indicate that the behavior of phonons in MWCNT is dominated by boundary and point-defect scattering rather than the three-phonon Umklapp process.

first peeled sample is not a perfect circle and the diameter is overestimated, and consequently, \dot{q} , k and ρ are underestimated; (2) the peeling process made the first sample looser than the whole rope. Using this density, the specific heat from 300 K to 800 K is calculated, as plotted in Fig. 8b against $c_p(T)$ of graphite and MWCNTs [26]. The figure shows that c_p of MWCNTs above 300 K is lower than that of graphite.

3.3. Analysis of the tube-to-tube thermal contact resistance

The above obtained k for these MWCNT bundles is in the order of 10 W/m K, which is two to three orders of magnitude lower than the value for an individual CNT predicted theoretically [30,31] and measured experimentally [11,18]. Many authors attribute the significant difference to the large thermal contact resistance of the tube-to-tube junctions in bulk CNT samples compared with the intrinsic thermal resistance of an individual CNT. Based on this, an equation was developed

by using the atomistic Green's function approach to describe the relationship between the bulk thermal conductivity k and the interfacial thermal conductance σ at tube-to-tube junctions as $k \approx 0.09\sigma l / (\pi d \rho_{\text{graphene}})$ for SWCNT bundles [38], where l is the curvature length of the tube between two adjacent contact points, $\rho_{\text{graphene}} = 7.6 \times 10^{-7} \text{ kg}/\text{m}^2$ is the surface mass density of graphene, ρ and d are the density of bulk CNT and diameter of a single tube, respectively. A corresponding correlation for MWCNT samples was also established by our group [8] as $k \sim 2\sigma l \rho / \rho_g [\pi(d_1^2 - d_2^2) \rho_g]$, where d_1 and d_2 are the outer and inner diameter of the MWCNT, respectively. ρ_g is the volumetric density of graphene which is equal to $7.6 \times 10^{-7} / (3.4 \times 10^{-10}) = 2235 \text{ kg}/\text{m}^3$. SEM and TEM images of the samples are obtained to characterize the structure and diameters of the CNTs. Typical SEM images of the samples are shown at different magnifications in Fig. 9a and b. Although the MWCNTs are wave-like, the alignment is very noticeable and the direction of the waves follows the axial direction of the bundle. The typical outer diameter of the individual MWCNT in the sample is 18–26 nm and the wall number is typically in the range from 12 to 18, as shown in the TEM images Fig. 9c and d. The average outer and inner diameter of the individual tube is statistically calculated at 21 and 15 nm from considerable sampling measurements on many TEM images of different areas. The thermal conductance σ of CNT–CNT contact was computed as 10–100 pW/K for different chiralities [38]. With a typical $\rho = 200 \text{ kg}/\text{m}^3$ and $k = 9 \text{ W}/\text{m}\cdot\text{K}$, the mean curvature length of two adjacent tube contact points is estimated in the range of 340–3400 μm using $k \sim 2\sigma l \rho / \rho_g [\pi(d_1^2 - d_2^2) \rho_g]$. The thermal conductance G of a MWCNT in such length is calculated by $G = kA/l$ at about 100–1000 pW/K assuming the intrinsic thermal conductivity of MWCNT is 2000 W/m K. This thermal conductance is much larger than that of the CNT contact point, which means that the tube-to-tube thermal contact resistance is dominant in thermal transport in MWCNT bundles.

According to the kinetic theory, the phonon mean free path (MFP) l in bulk materials can be calculated from $k = Cv/3$, where C is the heat capacity per unit volume, and v is the phonon group velocity. It also can be represented by $l = 3\alpha/v$. It should be pointed out that the thermal transport in MWCNT bundles is dominated by the thermal contact resistance. Given the effective k value, the obtained l is not real phonon MFP in tubes and it is only the effective one in the bundles. Thus, taking the phonon group velocity at about $10^4 \text{ m}/\text{s}$ [28], the effective phonon MFP is about 20 nm for the first sample and about 13 nm for the second sample at room temperature. It is an order of magnitude lower than the intrinsic phonon MFP in individual CNTs. $l(T)$ will simply follow the same temperature dependence as the thermal diffusivity.

3.4. Effect of radiation heat loss

Previous work on the laser flash method for measuring the thermal diffusivity of a disk-shape sample indicated that the radiation heat loss plays an important role at high temperature measurement [29]. The radiation heat loss from the wire surface may also be critical in the GET technique, although the convection heat loss is reduced to be negligible

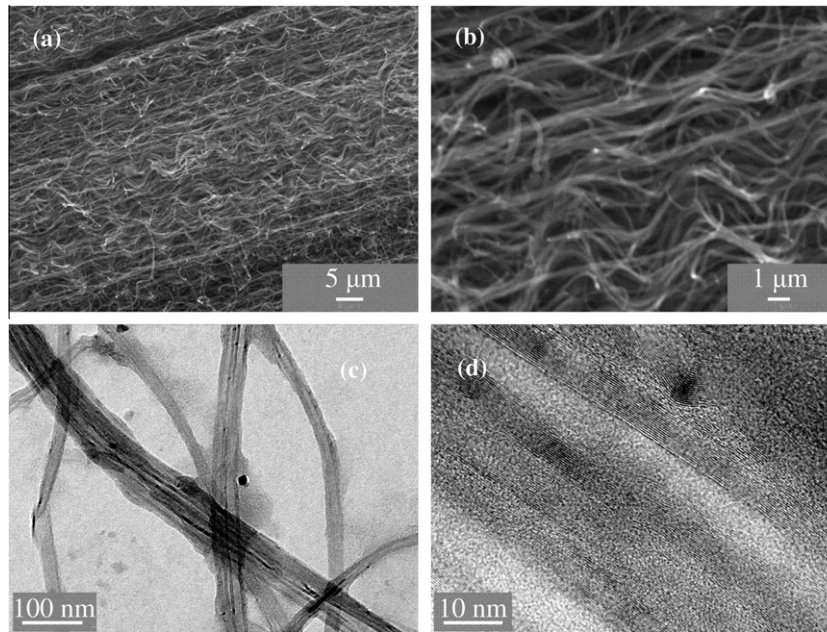


Fig. 9 – SEM and TEM images illustrating the aligned MWCNT bundles.

by placing the system in high vacuum chamber. The radiation heat loss from the wire surface induced by the self-heating of probing current is approximated by $q_{\text{rad}} = \varepsilon\sigma\pi dL[(T_0 + \Delta T)^4 - T_0^4]$, where ε is the emissivity, σ the Stefan–Boltzmann constant $5.67 \times 10^{-8} \text{ W m}^{-2} \text{ K}^{-4}$, d the diameter, L the length, and ΔT the average temperature rise over the sample. Meanwhile, the heat generation is $q_{\text{gen}} = A_c \dot{q}L$. With $\Delta T = \dot{q}L^2/12k$, the ratio η of radiation to heat generation is estimated as

$$\eta = \frac{q_{\text{rad}}}{q_{\text{gen}}} = \frac{\varepsilon\sigma\pi dL(4T_0^3\Delta T + 6T_0^2\Delta T^2 + 4T_0\Delta T^3 + \Delta T^4)}{A_c \dot{q}L} \approx \frac{4\varepsilon\sigma L^2 T_0^3}{3kd} \quad (2)$$

The approximation is valid when $\Delta T \ll T_0$. This radiation and generation estimation is for the steady state of the wire with a uniform heat generation inside. For the transient state, the ratio is smaller due to gradually increasing temperature. Thus the radiation has less effect on the thermal diffusivity than on the thermal conductivity and the ratio in Eq. (2) is the upper bound value. From Eq. (2), it is seen that the radiation effect is sample-dependent. A longer sample with a smaller diameter will have a larger radiation heat loss. Here, the first thin MWCNT bundle measured by GET 1 with a 4 mA current is taken for example. The average temperature increase is no more than 12 K which is much less than the lowest ambient temperature 300 K. The emissivity of carbon materials is close to 1. For extreme situation with $\varepsilon = 1$, the ratio η is 4.1% with $k = 5.83 \text{ W/m K}$ at $T_0 = 300 \text{ K}$ and 8.4% with $k = 7.11 \text{ W/m K}$ at $T_0 = 400 \text{ K}$. Since the ratio is much less than 1, the radiation heat loss is negligible for the measurement of the first sample. Eq. (2) also shows the initial temperature T_0 is an important factor to evaluate the radiation effect. If T_0 is higher, the ratio η could be larger and the radiation heat loss cannot be neglected. For the second sample measured by the GET 2 technique with 10 mA probing current, a large base current can heat up the sample by hundreds of Kelvin,

which will affect the ratio significantly. The maximum ratio is 15.5% with $k = 9 \text{ W/m K}$ at $T_0 = 800 \text{ K}$. This large ratio means that the radiation effect at high initial temperatures is noticeable and the corresponding k is overestimated in previous calculations. Thus, the real curves of $\alpha(T)$ and $k(T)$ should be lower at high temperatures from the measured ones shown in Fig. 8a. Considering the large variety of existing measured thermal conductivity, a ratio 10% with $k = 9 \text{ W/m K}$ at $T_0 = 700 \text{ K}$ is an acceptable uncertainty. For other materials with very low emissivity and high thermal conductivity such as metals, the radiation heat loss should be much lower than the above values. This analysis calls attention to the consideration of radiation heat loss when measuring the thermal properties of micro/nano wires at high temperatures, especially individual CNTs due to the extremely high aspect ratio.

4. Conclusion

In this work we report on two different techniques for measuring the thermophysical properties of MWCNT bundles. An extended technique GET 2 based on the GET 1 technique was developed to evaluate the thermophysical properties of wire-samples at elevated temperatures. From measurements of two samples with different diameter and length, the results show that the feeding current has negligible effect on the thermophysical properties of the MWCNT bundles. The thermal diffusivity α and thermal conductivity k at room temperature are $6 \times 10^{-5} \text{ m}^2/\text{s}$ and 5.8 W/m K for the first MWCNT bundle, $4.6 \times 10^{-5} \text{ m}^2/\text{s}$ and 7.6 W/m K for the second bundle, respectively. The obtained k is larger than the reported values of unaligned bundles and arrays and comparable to the reported data of aligned ones. Compared with the experimental and theoretical values of individual CNTs, the two magnitude lower k also illustrates that the thermal transport in CNT bundles is dominated by the thermal contact resistance of tube-

to-tube contacts. The effective density of the two MWCNT bundles was measured at 116 kg/m^3 and 234 kg/m^3 , respectively. The possible reasons for the difference are the uncertainty in cross-sectional area calculation for the first sample and structure looseness induced by the peeling process. The temperature dependence of α and k at temperatures up to 830 K was studied. α decreased and k increased slightly with temperature. Unlike the decreasing k at high temperatures for many solid materials, the increasing k at high temperatures for the MWCNT bundles indicates that the dominant phonon scattering mechanism is boundary and point-defect scattering instead of three-phonon Umklapp scattering. The specific heat c_p above room temperature was evaluated for the first time. It is seen that the behavior of $c_p(T)$ for CNTs is close to graphite at 300–400 K but lower than that for graphite above 400 K, indicating a higher Debye temperature. Thus, the phonons at very high frequencies (optical phonons) in MWCNTs also contribute to thermal energy storage. The presence of some optical phonons also implies that the behavior of phonons in MWCNTs is dominated by boundary and point-defect scattering rather than the three-phonon Umklapp scattering. The thermal contact resistance at tube-to-tube junctions in bulk CNT samples results in significant k reduction. The mean curvature length of two adjacent tube contacts in these bundles was estimated in the order of micrometer to millimeter. The analysis of radiation heat loss shows that it needs to be considered when studying the thermal transport in micro/nano wires at high temperatures, especially for individual CNTs due to their extremely high aspect ratio.

Acknowledgments

The authors wish to thank Yanan Yue for the help on the Raman spectra experiment. We also gratefully acknowledge the support of the National Science Foundation (CBET-0931290 and CMMI-0926704). Partial support from the start-up fund of Iowa State University is gratefully acknowledged. Part of this research (MWCNT synthesis by GE) was sponsored by the Materials Sciences and Engineering Division, Office of Basic Energy Sciences, US Department of Energy.

REFERENCES

- [1] Harris PJF. Carbon nanotube science: synthesis, properties and applications. 2nd ed. New York: Cambridge University Press; 2009.
- [2] Hone J, Llaguno MC, Nemes NM, Johnson AT, Fischer JE, Walters DA, et al. Electrical and thermal transport properties of magnetically aligned single wall carbon nanotube films. *Appl Phys Lett* 2000;77(5):666–8.
- [3] Borca-Tasciuc T, Vafaei S, Borca-Tasciuc DA, Wei BQ, Vajtai R, Ajayan PM. Anisotropic thermal diffusivity of aligned multiwall carbon nanotube arrays. *J Appl Phys* 2005;98(5):054309–14.
- [4] Ivanov I, Poretzky A, Eres G, Wang H, Pan ZW, Cui HT, et al. Fast and highly anisotropic thermal transport through vertically aligned carbon nanotube arrays. *Appl Phys Lett* 2006;89(22):223110–2.
- [5] Xu Y, Zhang Y, Suhir E, Wang XW. Thermal properties of carbon nanotube array used for integrated circuit cooling. *J Appl Phys* 2006;100(7):074302–6.
- [6] Xie HQ, Cai A, Wang XW. Thermal diffusivity and conductivity of multiwalled carbon nanotube arrays. *Phys Lett A* 2007;369(1–2):120–3.
- [7] Wang D, Song PC, Liu CH, Wu W, Fan SS. Highly oriented carbon nanotube papers made of aligned carbon nanotubes. *Nanotechnology* 2008;19(7):075604–9.
- [8] Yue YN, Huang XP, Wang XW. Thermal transport in multiwall carbon nanotube buckypapers. *Phys Lett A* 2010;374(40):4144–51.
- [9] Jakubinek MB, White MA, Li G, Jayasinghe C, Cho W, Schulz MJ, et al. Thermal and electrical conductivity of tall, vertically aligned carbon nanotube arrays. *Carbon* 2010;48(13):3947–52.
- [10] Yi W, Lu L, Zhang DL, Pan ZW, Xie SS. Linear specific heat of carbon nanotubes. *Phys Rev B* 1999;59(14):R9015–8.
- [11] Kim P, Shi L, Majumdar A, McEuen PL. Thermal transport measurements of individual multiwalled nanotubes. *Phys Rev Lett* 2001;87(21):215502–5.
- [12] Shi L, Li DY, Yu CH, Jang WY, Kim D, Yao Z, et al. Measuring thermal and thermoelectric properties of one-dimensional nanostructures using a microfabricated device. *J Heat Transfer-Trans ASME* 2003;125(5):881–8.
- [13] Guo JQ, Wang XW, Wang T. Thermal characterization of microscale conductive and nonconductive wires using transient electrothermal technique. *J Appl Phys* 2007;101(6):063537–43.
- [14] Jin R, Zhou ZX, Mandrus D, Ivanov IN, Eres G, Howe JY, et al. The effect of annealing on the electrical and thermal transport properties of macroscopic bundles of long multi-wall carbon nanotubes. *Phys B: Condensed Matter* 2007;388(1–2):326–30.
- [15] Yue YN, Eres G, Wang XW, Guo LY. Characterization of thermal transport in micro/nanoscale wires by steady-state electro-Raman-thermal technique. *Appl Phys A – Mater Sci Process* 2009;97(1):19–23.
- [16] Guo JQ, Wang XW, Geohegan DB, Eres G, Vincent C. Development of pulsed laser-assisted thermal relaxation technique for thermal characterization of microscale wires. *J Appl Phys* 2008;103(11):113505–13.
- [17] Aliev AE, Guthy C, Zhang M, Fang S, Zakhidov AA, Fischer JE, et al. Thermal transport in MWCNT sheets and yarns. *Carbon* 2007;45(15):2880–8.
- [18] Fujii M, Zhang X, Xie HQ, Ago H, Takahashi K, Ikuta T, et al. Measuring the thermal conductivity of a single carbon nanotube. *Phys Rev Lett* 2005;95(6):065502–5.
- [19] Yu CH, Shi L, Yao Z, Li DY, Majumdar A. Thermal conductance and thermopower of an individual single-wall carbon nanotube. *Nano Lett* 2005;5(9):1842–6.
- [20] Pop E, Mann D, Wang Q, Goodson K, Dai HJ. Thermal conductance of an individual single-wall carbon nanotube above room temperature. *Nano Lett* 2006;6(1):96–100.
- [21] Wang ZL, Tang DW, Li XB, Zheng XH, Zhang WG, Zheng LX, et al. Length-dependent thermal conductivity of an individual single-wall carbon nanotube. *Appl Phys Lett* 2007;91(12):123119–21.
- [22] Zhang HL, Li JF, Yao KF, Chen LD. Spark plasma sintering and thermal conductivity of carbon nanotube bulk materials. *J Appl Phys* 2005;97(11):114310–4.
- [23] Zhang HL, Li JF, Zhang BP, Yao KF, Liu WS, Wang H. Electrical and thermal properties of carbon nanotube bulk materials: experimental studies for the 328–958 K temperature range. *Phys Rev B* 2007;75(20):205407–15.
- [24] Li JL, Wang LJ, He T, Jiang W. Transport properties of hot-pressed bulk carbon nanotubes compacted by spark plasma sintering. *Carbon* 2009;47(4):1135–40.

- [25] Mizel A, Benedict LX, Cohen ML, Louie SG, Zettl A, Budraa NK, et al. Analysis of the low-temperature specific heat of multiwalled carbon nanotubes and carbon nanotube ropes. *Phys Rev B* 1999;60(5):3264–70.
- [26] Masarapu C, Henry LL, Wei BQ. Specific heat of aligned multiwalled carbon nanotubes. *Nanotechnology* 2005;16(9):1490–4.
- [27] Incropera FP, DeWitt DP, Bergman TL, Lavine AS. *Fundamentals of heat and mass transfer*. 6th ed. New York: John Wiley and Sons, Inc.; 2007.
- [28] Dresselhaus MS, Eklund PC. Phonons in carbon nanotubes. *Adv Phys* 2000;49(6):705–814.
- [29] Cowan RD. Pulse method of measuring thermal diffusivity at high temperatures. *J Appl Phys* 1963;34(4):926–7.
- [30] Berber S, Kwon Y-K, Tománek D. Unusually high thermal conductivity of carbon nanotubes. *Phys Rev Lett* 2000;84(20):4613–6.
- [31] Osman MA, Srivastava D. Temperature dependence of the thermal conductivity of single-wall carbon nanotubes. *Nanotechnology* 2001;12(1):21–4.
- [32] Kitsuki H, Yamada T, Fabris D, Jameson JR, Wilhite P, Suzuki M, et al. Length dependence of current-induced breakdown in carbon nanofiber interconnects. *Appl Phys Lett* 2008;92(17):173110–2.
- [33] Moser J, Barreiro A, Bachtold A. Current-induced cleaning of graphene. *Appl Phys Lett* 2007;91(16):163513–5.
- [34] Wang X, Li X, Zhang L, Yoon Y, Weber PK, Wang H, et al. N-doping of graphene through electrothermal reactions with ammonia. *Science* 2009;324(5928):768–71.
- [35] Eres G, Poretzky AA, Geohegan DB, Cui H. In situ control of the catalyst efficiency in chemical vapor deposition of vertically aligned carbon nanotubes on predeposited metal catalyst films. *Appl Phys Lett* 2004;84(10):1759–61.
- [36] Shaffer MSP, Fan X, Windle AH. Dispersion and packing of carbon nanotubes. *Carbon* 1998;36(11):1603–12.
- [37] Zhang M, Fang SL, Zakhidov AA, Lee SB, Aliev AE, Williams CD, et al. Strong, transparent, multifunctional, carbon nanotube sheets. *Science* 2005;309(5738):1215–9.
- [38] Chalopin Y, Volz S, Mingo N. Upper bound to the thermal conductivity of carbon nanotube pellets. *J Appl Phys* 2009;105(8):084301–12.